Available online at www.sciencedirect.com
SCIENCE DIRECT®
Journal of Nuclear Materials 351 (2006) 187–196
journal of nuclear materials
www.elsevier.com/locate/jnucmat

APT characterization of high nickel RPV steels

M.K. Miller *, M.A. Sokolov, R.K. Nanstad, K.F. Russell

Microscopy, Microanalysis, Microstructure Group, Metals and Ceramics Division, Oak Ridge National Laboratory, P.O. Box 2008, Building 4500S, MS 6136, Oak Ridge, TN 37831-6136, USA

Abstract

The microstructures of three high nickel content pressure vessel steels have been characterized by atom probe tomography to investigate the influence of high nickel levels on the response to neutron irradiation of high and low copper pressure vessel steels. The high-nickel, low-manganese, low-copper VVER-1000 weld and forging exhibited lower than predicted levels of embrittlement during neutron irradiation. The Palisades weld exhibits a $\Delta T_{41\,J}$ of 102 °C which was significantly lower than the value of 154 °C predicted by Reg. Guide 1.99 Rev. 2. Atom probe tomography revealed nickel-, manganese-, and silicon-enriched precipitates in both the VVER-1000 base and weld materials after neutron irradiation. A high number density of copper-, nickel-, manganese-, silicon- and phosphorus-enriched precipitates were observed in the Palisades weld after neutron irradiation. Atom probe tomography also revealed high levels of phosphorus segregation to the dislocations in all three materials.
Published by Elsevier B.V.

PACS: 61.82.Bg; 62.20.Mk; 81.40.−z

1. Introduction

Nickel is added to reactor pressure vessel (RPV) steels to increase hardenability and decrease the ductile-brittle transition temperature. It is generally accepted that the presence of nickel in RPV steels also increases their sensitivity to neutron induced embrittlement even at low phosphorus and copper concentrations [1–3]. Based on mechanical properties data alone, it is difficult to rationalize data that appear to conflict with those observations. The mechanisms controlling the damage process are not well understood, although microstructural studies of irradiated RPV steels have shown clear evidence of nickel in the irradiation-induced copper-enriched precipitates, a copper–nickel synergistic effect and, more recently, a nickel–manganese synergistic effect [4–8].

However, there is only a limited amount of data on neutron embrittlement of RPV steels with relatively high nickel content, and especially for VVER-1000 steels (Ni–Cr–Mo–V) with very high nickel content. Because of the significance of transition temperature shift predictions for RPV integrity assessments, it is of great importance to investigate the mechanisms of neutron embrittlement of

* Corresponding author. Tel.: +1 865 574 4719; fax: +1 865 241 3650.
E-mail address: millermk@ornl.gov (M.K. Miller).

0022-3115/$ - see front matter Published by Elsevier B.V.
doi:10.1016/j.jnucmat.2006.02.013

light-water RPV steels containing high nickel contents, especially weld metals, including those typical of pressurized water reactor (PWR) RPVs (Mn–Ni–Cr–Mo). To quantify these effects, the irradiation-induced physical changes in the microstructures of the steels can be identified using state-of-the-art analytical techniques and these observations can be correlated with the observed changes in mechanical properties.

In this study, the microstructures of three high nickel content pressure vessel steels have been characterized by atom probe tomography [9,10]. This technique has been used to characterize several neutron irradiated RPV steels and model alloys [11–23].

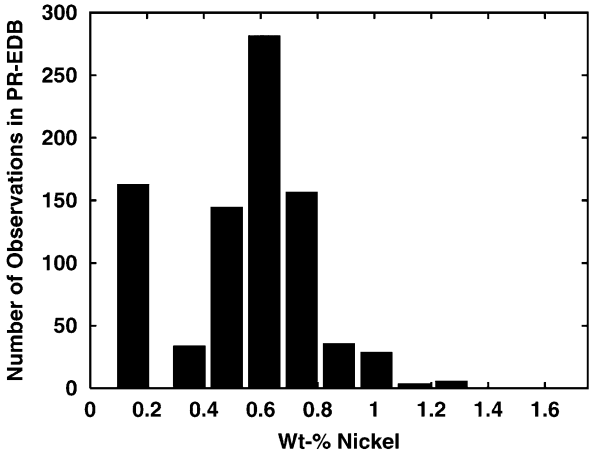

Fig. 1. The number of steels in the PR-EDB data base as a function of nickel content. The nickel contents of the VVER-1000 forging, VVER-1000 weld and the Palisades weld were 1.26, 1.78 and 1.20 wt% Ni, respectively.

The purposes of this study were to investigate the influence of high nickel levels on the response to neutron irradiation of high and low copper pressure vessel steels and to establish whether any additional phases were present after neutron irradiation. The nickel levels in these steels (1.20–1.78% Ni) were at least twice that typically found (~0.6% Ni) in most Western pressure vessel steels, as compared to the steels in the Power Reactor Embrittlement Data Base (PR-EDB) [24] shown in Fig. 1.

2. Experimental

Two different types of pressure vessel steels with low and high copper contents were selected for this study. The first set of alloys consisted of a low copper (~0.05% Cu) forging (15Kh2NMFAA) and a weld metal (weld wire 12Kh2N2MAA) used in a VVER-1000 reactor. The full compositions of the lower nickel (1.26% Ni, 0.05% Cu) VVER-1000 forging and the higher nickel (1.78% Ni, 0.07% Cu) VVER-1000 weld metal are given in Table 1. The VVER-1000 forging was austenitized at 920 °C, water quenched, tempered at 650 °C and furnace cooled. The VVER-1000 submerged-arc weld was post weld heat treated at 620 °C for 25 h and furnace cooled. The vessel was then stress relieved at 650 °C for 20 h and furnace cooled. The VVER-1000 steels were irradiated in the HSSI Program's irradiation facilities at the University of Michigan, Ford Nuclear Reactor at a temperature of 288 °C for 2137 h at an average flux of 7.08×10^{11} cm^{-2} s^{-1} for a fluence of 5.45×10^{22} n m^{-2} ($E > 1$ MeV) and for 5340 h at an average flux of 4.33×10^{11} cm^{-2} s^{-1} for a fluence of 8.32×10^{22} n m^{-2} ($E > 1$ MeV).

Table 1
Compositions of the steels used in this study

Element	VVER-1000 reactor				Palisades reactor	
	Forging		Weld		Weld	
	wt%	at.%	wt%	at.%	wt%	at.%
Cu	0.05	0.04	0.07	0.06	0.20	0.18
Ni	1.26	1.19	1.78	1.69	1.20[a]	1.14
Mn	0.46	0.46	0.80	0.81	1.27	1.29
Si	0.30	0.59	0.33	0.65	0.18	0.36
Cr	2.2	2.34	1.80	1.93	0.04	0.04
Mo	0.51	0.30	0.59	0.33	0.55	0.32
V	0.10	0.11	–	–	0.003	0.003
C	0.17	0.78	0.06	0.28	0.11	0.51
P	0.008	0.014	0.005	0.009	0.014	0.03

The balance is iron.
[a] Nickel level limit of Reg. Guide 1.99 Rev. 2.

Therefore, the total fast fluence was 1.38×10^{23} n m^{-2} ($E > 1$ MeV).

The second type of pressure vessel steel was a high copper (0.20 wt% Cu), high nickel (1.2 wt% Ni) weld from the Palisades reactor. The average composition of the Palisades weld is listed in Table 1. The nickel level in the Palisades weld (1.20 wt%) is the maximum nickel level permitted for predicting a shift in the transition temperature under Reg. Guide 1.99 Rev. 2. This steam generator weld was fabricated with a submerged-arc welding process with weld wire (heat 34B009) with a nickel addition

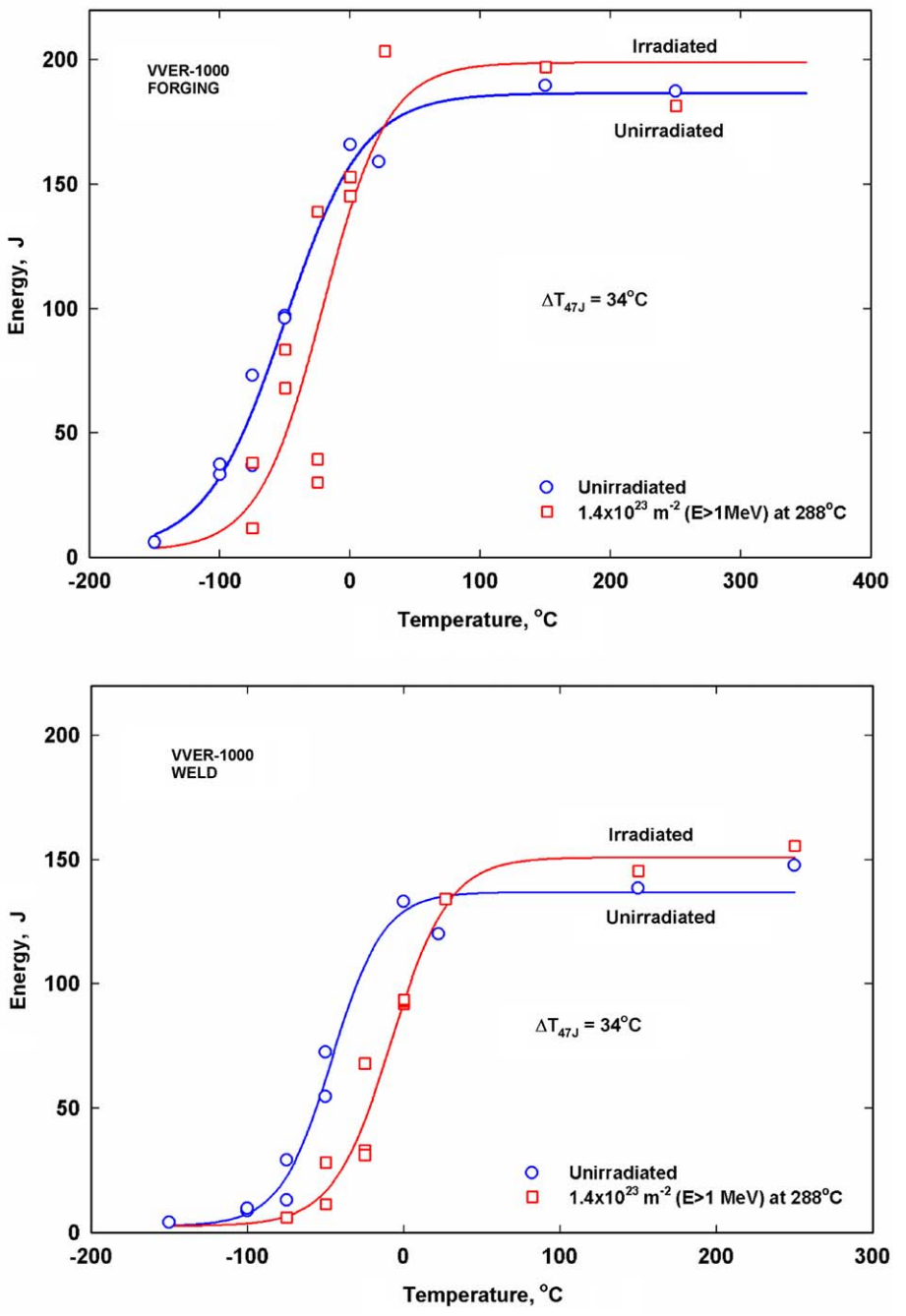

Fig. 2. Ductile-to-brittle transition curves of the unirradiated and neutron irradiated VVER-1000 forging and weld materials.

(Ni-200 heat number N7753A), and a Linde 1092 welding flux (Lot No. 3708). It was post weld heat treated in the range 593–627 °C for ~14 h. The Palisades weld was also irradiated in the Ford reactor at a temperature of 288 °C and a flux of $\sim 7 \times 10^{11}$ cm^{-2} s^{-1} to a fluence of 1.4×10^{23} n m^{-2} ($E > 1$ MeV).

These three alloys were characterized with the Oak Ridge National Laboratory's local electrode atom probe. A specimen temperature of 50 K, a pulse repetition rate of 200 kHz and a pulse fraction of 20% were used for the analyses. The high pulse repetition rate of this instrument significantly reduces the possibility of preferential evaporation of the low evaporation field solutes such as copper [10,25].

The presence of the solute-enriched precipitates and the compositions of their cores were determined with the maximum separation envelope method [9,14]. This method is based on the premise that the distance between solute atoms in a solute-enriched precipitate is significantly smaller than that in the surrounding matrix. Therefore, the solute atoms that belong to a solute-enriched precipitate may be distinguished from those in the matrix based on a maximum separation distance, d_{max}. The size of the solute-enriched features was estimated in terms of the Guinier radius, which was determined from positions of the solute atoms in each precipitate [9]. The solute atom positions defined by the maximum separation method were also used to define the extent of each precipitate by marking cells in a fine three-dimensional grid with a grid spacing of 0.1 nm. The composition of the precipitate was then determined from the number of all the atoms in these marked cells. At the size range of the precipitates in these RPV steels (i.e., <5 nm diameter), the definition of the extent of the precipitate and solute gradients at the precipitate–matrix interface have strong influences on the composition estimates. The number densities were estimated from the number of particles in the volume of analysis, where the volume was estimated from the number of atoms in the volume, the detection efficiency of the mass spectrometer and the atomic density of body centered cubic iron [9].

3. Results

3.1. Mechanical properties

The Charpy v-notch impact ductile-to-brittle transition curves using a tanh fitting function for the unirradiated and neutron irradiated VVER-1000 forging and weld are shown in Fig. 2. Both the VVER-1000 forging and weld exhibit $\Delta T_{41\,J}$

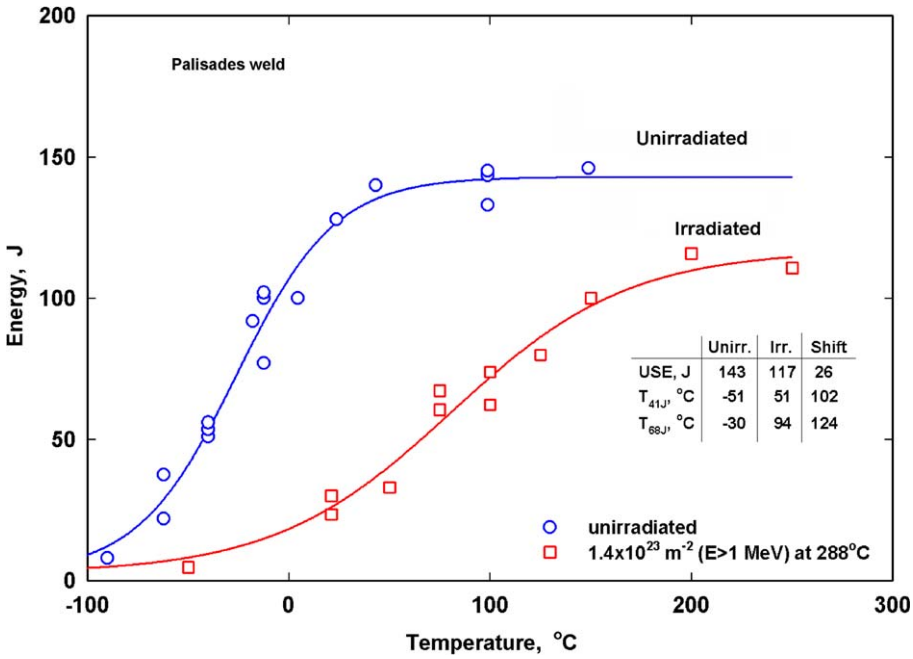

Fig. 3. Ductile-to-brittle transition curves for the unirradiated and neutron irradiated Palisades weld.

values of 34 °C. The typical 95% confidence limits of these $\Delta T_{41\,\mathrm{J}}$ values are ~10 °C [26,27]. Values of 57 and 66 °C, respectively for the forging and weld were predicted from the Russian norm regulatory guidelines based on the fluence, phosphorus and copper contents of the alloys. Therefore, the high-nickel, low-manganese, low-copper VVER-1000 weld and forging exhibited lower than predicted levels of embrittlement during neutron irradiation [28].

The Charpy v-notch impact ductile-to-brittle transition curves using a tanh fitting function for the unirradiated and neutron irradiated high nickel Palisades A533B weld is shown in Fig. 3. The upper shelf energies of the unirradiated and neutron irradiated materials were 143 and 117 J, respectively. The $T_{41\,\mathrm{J}}$ values of the unirradiated and neutron irradiated weld materials were −51 and 51 °C, respectively. The $T_{68\,\mathrm{J}}$ values of the unirradiated and neutron irradiated weld materials were −30 and 94 °C, respectively. Therefore, the Palisades weld exhibits a mean $\Delta T_{41\,\mathrm{J}}$ shift of 102 °C. This shift is significantly lower than the value of 154 °C predicted by the Reg. Guide 1.99 Rev. 2 [29]. The Eason, Wright and Odette (EWO) [30] and ASTM E900 [31] parameters were both 137 °C.

3.2. Microstructure

Atom probe tomography revealed approximately spherical nickel-, manganese-, and silicon-enriched precipitates in both neutron irradiated VVER-1000 base and weld materials, as shown in the atom maps in Figs. 4 and 5, respectively. These precipitates were difficult to distinguish in the static atom maps of the entire volume of analysis due to the relatively high levels of nickel, manganese and silicon in the matrix and the high density of precipitates through the projected thickness of the analyzed volume. Therefore, the atom maps shown in Figs. 4 and 5 are 2-nm-thick slices selected through the local electrode atom probe data. Selected volume analysis of a few of these precipitates in the VVER-1000 weld revealed an approximate composition of Fe–10–15% Ni, 4–6% Mn and 4–6% Si. The maximum separation method [9,14] was not effective at distinguishing these precipitates from the matrix due to the relatively high levels of nickel, manganese and silicon in the matrix and the Ni_{58}/Fe_{58} isobar overlap. The average diameter of these precipitates was estimated from their extent in the atom maps and was approximately 2–4 nm. The number density estimated in the VVER-1000 weld was $\sim 1.5 \times 10^{23}\ \mathrm{m}^{-3}$. The number density estimated in the forging was slightly lower, $\sim 1 \times 10^{23}\ \mathrm{m}^{-3}$. This trend is consistent with the higher nickel content and higher nickel supersaturation of this alloy. No significant copper enrichment was detected in the precipitates in these low copper alloys. No copper-enriched precipitates were observed in these alloys indicating that the 0.04 and 0.06 at.% copper in these VVER materials was at or below the supersaturation required for their formation during neutron irradiation. Therefore, the embrittlement observed in these materials resulted from the presence of the nickel-, manganese-, and silicon-enriched precipitates.

No fine precipitates were found in the matrix of the unirradiated Palisades weld and no depletion in the matrix copper content from 0.18 at.% Cu was detected. A high number density of approximately spherical copper-, nickel-, manganese-, silicon- and

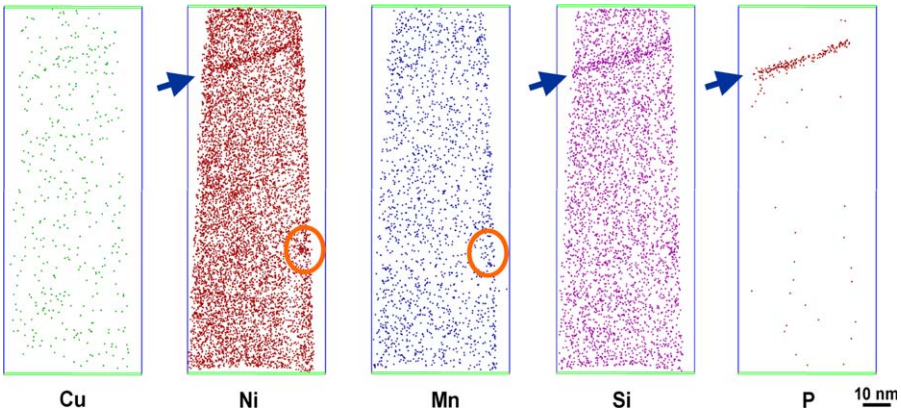

Fig. 4. Atom maps of the neutron irradiated VVER-1000 base material. A small nickel- and manganese-enriched precipitate is circled. A dislocation that is enriched in phosphorus, nickel and silicon is arrowed.

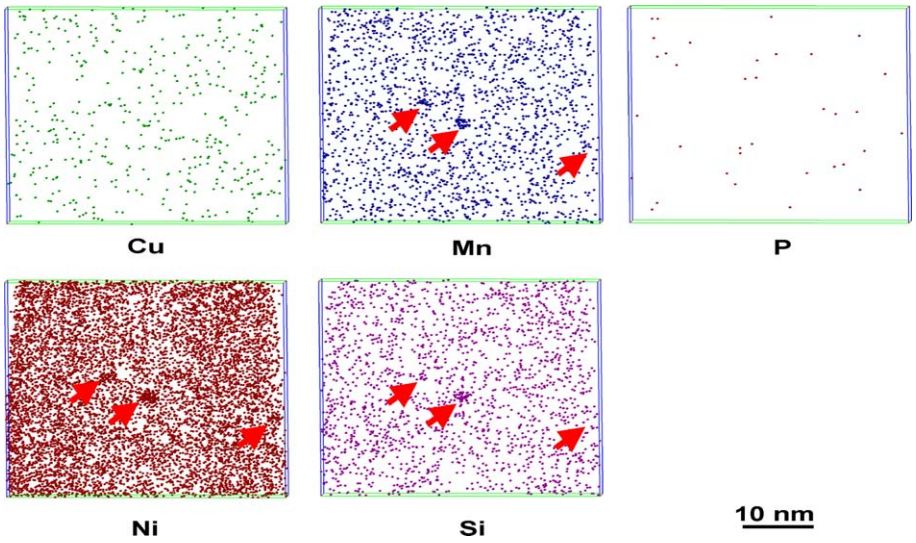

Fig. 5. Atom maps of the neutron irradiated VVER-1000 weld material showing some ultrafine manganese-, nickel- and silicon-enriched precipitates (arrowed).

phosphorus-enriched precipitates were observed in the neutron irradiated Palisades weld, as shown in Fig. 6. A higher magnification view of the solute associated with a single particle is shown in Fig. 7. The extents of the nickel, manganese, silicon and phosphorus atoms were larger than that of the copper atoms indicating some enrichment at the precipitate–matrix interface. The number density of these precipitates was estimated to be $N_v = 5 \times 10^{23}$ m^{-3} and their Guinier radius was $r_G = 0.9 \pm 0.2$ nm. The average number of copper atoms in these precipitates was approximately 50 ± 40 atoms. These precipitates were slightly smaller than the precipitates observed in other neutron irradiated RPV steels [11] indicating that the high nickel level may result in some retardation of their growth during irradiation. The compositions of 83 individual precipitates were estimated from the maximum separation envelope method [9] with a maximum separation distance of 0.6 nm and a grid spacing of 0.1 nm and are shown in Fig. 8. The average composition of the core of the precipitates was Fe–87 ± 8% Cu, 0.42% Mn, 0.77% Ni, 0.23% Si, 0.15 at.% P. The copper in solid solution in the ferrite matrix was estimated to be decreased to 0.07 ± 0.005 at.% Cu after neutron irradiation.

Atom probe tomography also revealed high levels of phosphorus segregation to the dislocations in all three materials. For example, dislocations in the neutron irradiated VVER-1000 base and Palisades

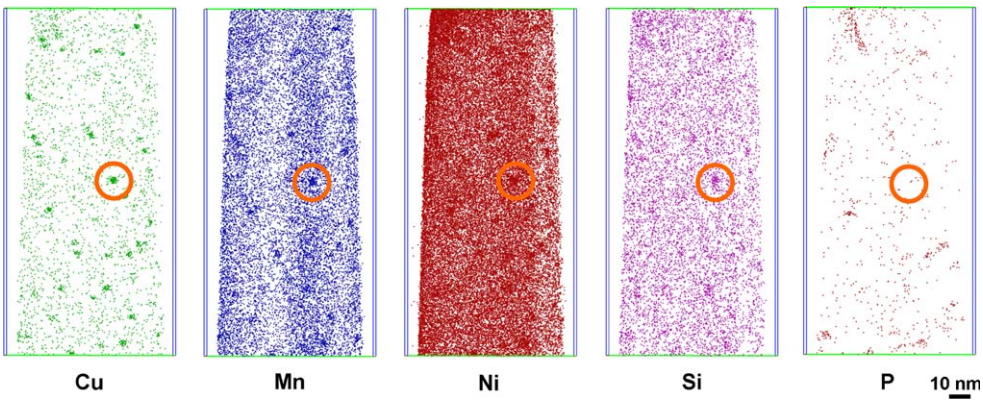

Fig. 6. Atom maps of the neutron irradiated Palisades weld material showing a high number density of ultrafine copper-, manganese-, nickel- and silicon-enriched precipitates.

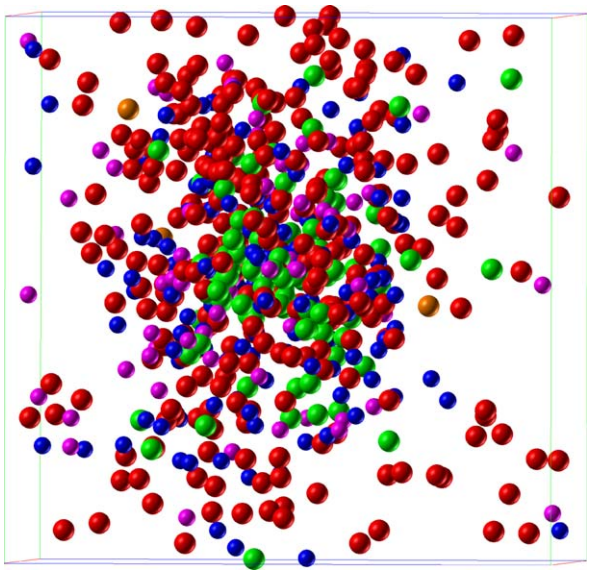

Fig. 7. Atom map of an ultrafine copper-, manganese-, nickel- and silicon-enriched precipitate in the neutron irradiated Palisades weld material. Copper atoms are green, manganese atoms are blue, nickel atoms are red, silicon atoms are purple and phosphorus atoms are orange. Box is $5 \times 5 \times 5$ nm. (For interpretation of the references in colour in this figure legend, the reader is referred to the web version of this article.)

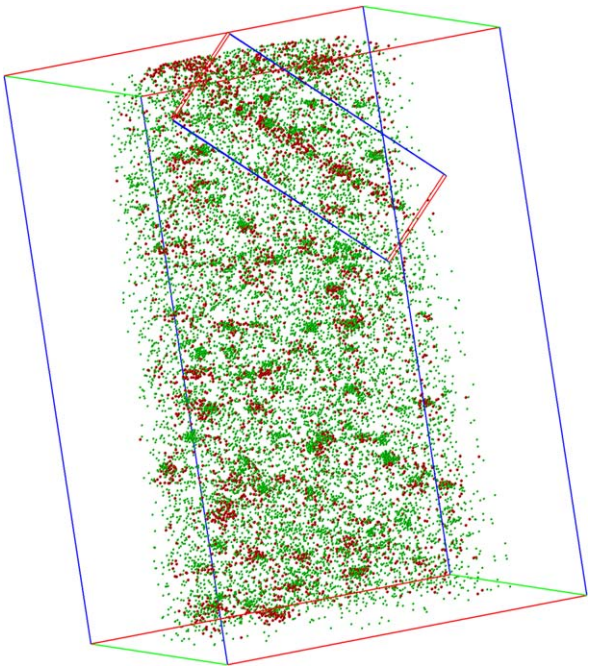

Fig. 9. Atom map of the neutron irradiated Palisades weld showing 83 copper-enriched precipitates and a dislocation with phosphorus segregation. The smaller box surrounding the dislocation is $20 \times 20 \times 50$ nm. Green atoms are copper, red atoms are phosphorus. (For interpretation of the references to color in this figure legend, the reader is referred to the web version of this article.)

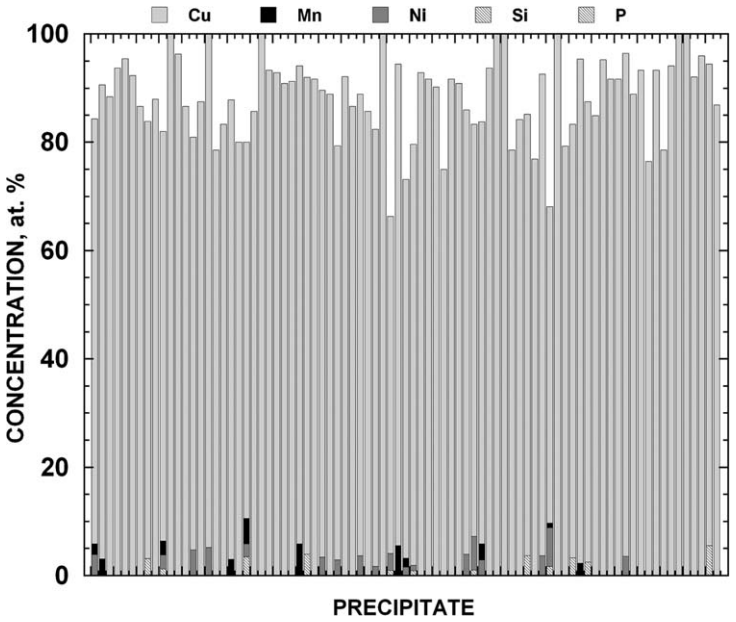

Fig. 8. Compositions of the core regions of the ultrafine copper-, manganese-, nickel- and silicon-enriched precipitates in neutron irradiated Palisades weld material. The balances of the compositions are iron.

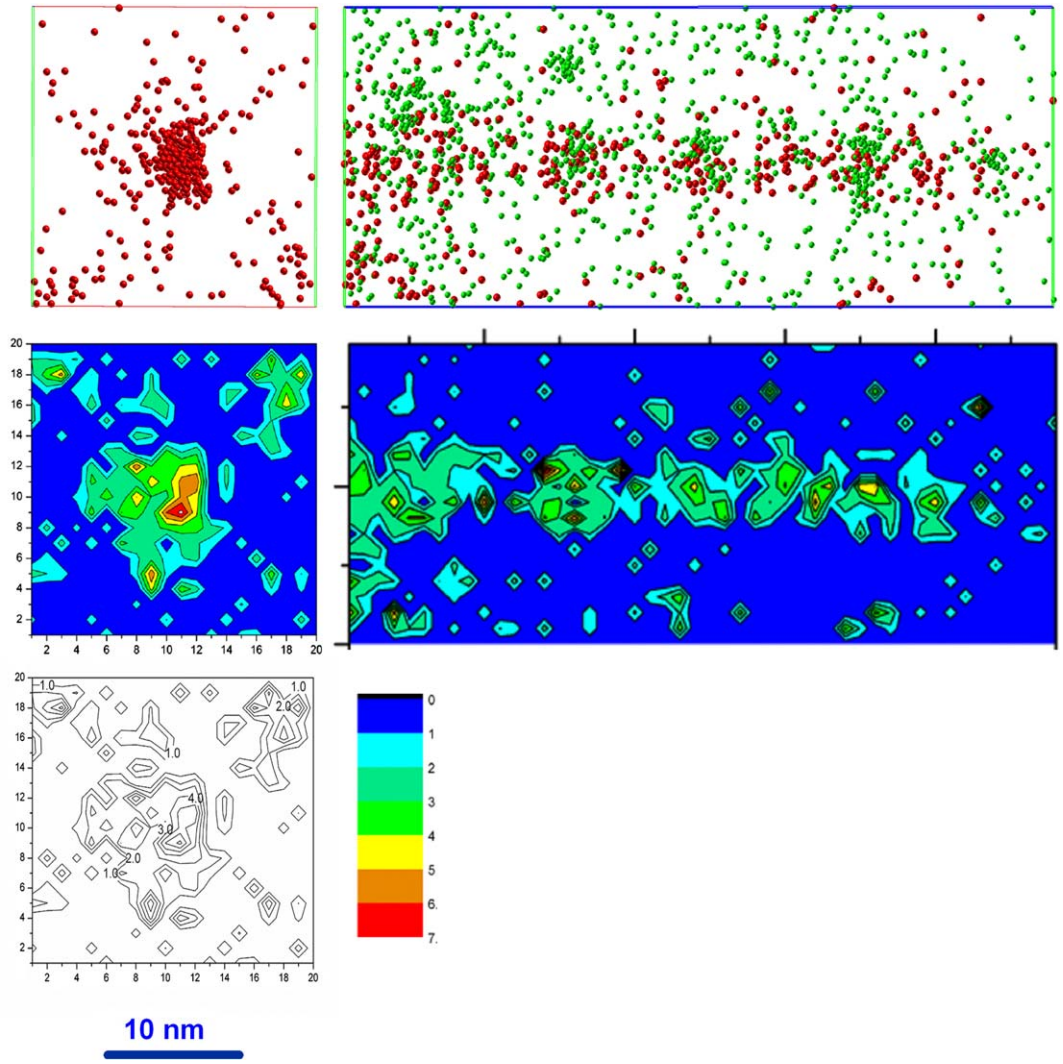

Fig. 10. Atom map and two-dimensional tracer maps of the box shown in Fig. 9 surrounding the dislocation. The views were constructed parallel to the core (left) and perpendicular to the core of the dislocation (right). The maximum phosphorus level was ~7 at.% P. Green atoms are copper, red atoms are phosphorus. (For interpretation of the references in colour in this figure legend, the reader is referred to the web version of this article.)

weld are shown in Figs. 4 and 9, respectively. Higher magnification views parallel and perpendicular to the core of the dislocation in the neutron irradiated Palisades weld are shown in Fig. 10. The lateral extent of the phosphorus segregation was estimated to be ~5 nm. The local phosphorus concentration was estimated with the tracer method. This method is analogous to taking an X-ray picture except that the two-dimensional intensity variation is related to the maximum concentration in projection through the thickness of the volume rather than the absorption of the X-rays. The volume encompassing a dislocation and some surrounding matrix (i.e., the selection box shown in Fig. 9) is divided into a three-dimensional array of volume elements, typically 1–2 nm on each side. The composition of each volume element is estimated. The volume element with the maximum phosphorus concentration is then found for each column of volume elements along one of the orthogonal directions. The concentrations of all the solutes in these volume elements may be displayed as two-dimensional contour map or solute intensity plot, as shown in Fig. 10. This tracer method indicates average levels of 3–4 at.% P with peaks of up to ~7 at.% P at the dislocation.

4. Conclusions

The low copper (~0.05 wt%) high nickel (1.26 and 1.78 wt% Ni) VVER-1000 forging and weld materials that were neutron irradiated to a total fluence of 1.38×10^{23} n m^{-2} ($E > 1$ MeV) exhibited lower than expected shifts in the ductile-to-brittle transition temperature of $\Delta T_{41\,J} = 34$ °C. Atom probe tomography revealed ultrafine nickel-, manganese-, and silicon-enriched precipitates but no copper-enriched precipitates. These observations support other studies that show a strong synergism of nickel and manganese in increasing the radiation sensitivity of RPV steels even for steels with low copper contents. The high copper (0.20 wt% Cu), high nickel (1.2 wt% Ni) Palisades weld that was neutron irradiated to a fast fluence of 1.4×10^{23} n m^{-2} ($E > 1$ MeV) exhibited a shift of $\Delta T_{41\,J} = 102$ °C. This shift is significantly lower than the value of 154 °C predicted by Reg. Guide 1.99 Rev. 2. Atom probe tomography revealed a high number density of ~2-nm-diameter copper-, nickel-, manganese-, silicon- and phosphorus-enriched precipitates in the neutron irradiated Palisades weld. Phosphorus segregation to dislocations was observed in all materials.

Acknowledgements

Research at the Oak Ridge National Laboratory SHaRE User Facility was sponsored by the Division of Materials Sciences and Engineering (MKM, KFR), US Department of Energy, under contract DE-AC05-00OR22725 with UT-Battelle, LLC and by the Office of Nuclear Regulatory Research, US Nuclear Regulatory Commission under inter-agency agreement DOE 1886-N695-3W with the US Department of Energy.

References

[1] A.M. Kryukov, Y.A. Nikolaev, A.V. Nikolaeva, Nucl. Eng. Des. 186 (1998) 353.
[2] T.J. Williams, P.R. Burtz, C.A. English, P.H.N. de la Cour Ray, in: G.J. Theus, J.R. Weeks (Eds.), 3rd International Symposium on Environmental Degradation of Materials in Nuclear Power Systems – Water Reactors 1987, 1988, p. 121.
[3] G.R. Odette, G.E. Lucas, in: L.E. Steele (Ed.), Irradiation Embrittlement of Reactor Pressure Vessel Steels: An International Review, ASTM STP 909, ASTM, 1986, p. 206.
[4] G.R. Odette, G.E. Lucas, The effect of nickel on irradiation hardening of pressure vessel steels, in: N.H. Packan, R.E. Stoller, A.S. Kumar (Eds.), Effects of Radiation on Materials: 14th International Symposium, ASTM STP 1046, vol. II, American Society for Testing and Materials, Philadelphia, 1990, p. 323.
[5] G.R. Odette, Radiation induced microstructural evolution in reactor pressure vessel steels, Microstructure of Irradiated Materials, in: MRS Symposium Proceedings, vol. 373, Pittsburgh, PA, 1995, p. 137.
[6] R. Gerard et al., In-service embrittlement of the pressure vessel welds at the Doel I and II nuclear power plants, in: Effects of Radiation on Materials: 17th International Symposium, in: David S. Gelles, Randy K. Nanstad, Arvind S. Kumar, Edward A. Little (Eds.), ASTM STP 1046, vol. II, American Society for Testing and Materials, 1996, p. 294.
[7] G.R. Odette, C.L. Liu, B.D. Wirth, On the composition and structure of nanoprecipitates in irradiated pressure vessel steels, Microstructure Evolution During Irradiation, in: MRS Soc Symposium Proceedings, vol. 439, Pittsburgh, 1997, p. 457.
[8] Y.A. Nikolaev et al., Radiation embrittlement and thermal annealing behavior of Cr–Ni–Mo reactor pressure vessel materials, J. Nucl. Mater. 226 (1995) 144.
[9] M.K. Miller, Atom Probe Tomography: Analysis at the Atomic Level, Kluwer Academic/Plenum, New York, NY, 2000.
[10] M.K. Miller, A. Cerezo, M.G. Hetherington, G.D.W. Smith, Atom Probe Field Ion Microscopy, Oxford University, Oxford, UK, 1996.
[11] M.K. Miller, P. Pareige, M.G. Burke, Mater. Charact. 44 (2000) 235.
[12] M.K. Miller, M.G. Hetherington, M.G. Burke, Metall. Trans. 20A (1989) 2651.
[13] M.K. Miller, P. Pareige, in: G.E. Lucas, L. Snead, M.A. KirkJr., R.G. Elliman (Eds.), Proc. MRS 2000 Fall Meeting, Symposium R: Microstructural Processes in Irradiated Materials, Boston, MA, November 27–30, 2000, vol. 650, Materials Research Society, Pittsburgh, PA, 2001, p. R6.1.1.
[14] J.M. Hyde, C.A. English, in: G.E. Lucas, L. Snead, M.A. KirkJr., R.G. Elliman (Eds.), Proc. MRS 2000 Fall Meeting, Symposium R: Microstructural Processes in Irradiated Materials, Boston, MA, November 27–30, 2000, vol. 650, Materials Research Society, Pittsburgh, PA, 2001, p. R6.6.1.
[15] M.K. Miller, K.F. Russell, P. Pareige, in: G.E. Lucas, L. Snead, M.A. KirkJr., R.G. Elliman (Eds.), Proc. MRS 2000 Fall Meeting, Symposium R: Microstructural Processes in Irradiated Materials, Boston, MA, November 27–30, 2000, vol. 650, Materials Research Society, Pittsburgh, PA, 2001, p. R3.15.1.
[16] M.K. Miller, K.F. Russell, J. Kocik, E. Keilova, J. Nucl. Mater. 282 (2000) 83.
[17] M.K. Miller, K.F. Russell, J. Kocik, E. Keilova, Micron 32 (2001) 749.
[18] M.K. Miller, S.S. Babu, M.A. Sokolov, R.K. Nanstad, S.K. Iskander, Mater. Sci. Eng. A 327 (2002) 76.
[19] M.K. Miller, M.A. Sokolov, R.K. Nanstad, S.K. Iskander, in: Proc. 10th Int. Conf. on Environmental Degradation of Materials in Nuclear Power Systems – Water Reactors, Lake Tahoe, NV, August 5–9, 2001, Pub. NACE, 2002.
[20] M.G. Burke, R.J. Stofanak, J.M. Hyde, C.A. English, W.L. Server, in: Proc. 10th Int. Conf. on Environmental Degradation of Materials in Nuclear Power Systems - Water Reactors, Lake Tahoe, NV, August 5–9, 2001, Pub. NACE, 2002.
[21] R.G. Carter, N. Soneda, K. Dohi, J.M. Hyde, C.A. English, W. Server, J. Nucl. Mater. 398 (2001) 211.

[22] P. Auger, P. Pareige, S. Welzel, J.C. Van Duysen, J. Nucl. Mater. 280 (2000) 331.
[23] J.M. Hyde, D. Ellis, C.A. English, T.J. Williams, Microstructural evolution in high nickel submerged arc weld, in: 20th Int. Conf. Effects of Radiation on Materials, in: S.T. Rosinski, M.L. Grossbeck, T.R. Allen, A.S. Kumar (Eds.), ASTM STP 1405, American Society for Testing and Materials, West Conshohocken, PA, 2001, p. 262.
[24] F.W. Stallmann, J.A. Wang, F.B.K. Kam, PR-EDB: Power Reactor Embrittlement Data Base, Version 2, NUREG/CR-4816, US Nuclear Regulatory Commission, 1994.
[25] M.K. Miller, K.F. Russell, Surf. Interface Anal., in press.
[26] R.K. Nanstad, D.E. McCabe, F.M. Haggag, K.O. Bowman, D.J. Downing, Statistical analyses of fracture toughness results for two irradiated high-copper welds, in: Effects of Radiation on Materials: 15th International Symposium, in: R.E. Stoller, A.S. Kumar, D.S. Gelles (Eds.), ASTM STP 1125, American Society for Testing and Materials, Philadelphia, 1992, p. 270.
[27] J.J. McGowan, R.K. Nanstad, A statistical analyses of fracture toughness of irradiated low-alloy steel plate and welds, in: Influence of Radiation on Material Properties: 13th International Symposium (Part II), in: F.A. Garner, HenagerJr., N. Igata (Eds.), ASTM STP 956, American Society for Testing and Materials, Philadelphia, 1987, p. 569.
[28] M.A. Sokolov, R.K. Nanstad, Comparison of irradiation-induced shifts of K_{Jc} and Charpy impact toughness for reactor pressure vessel steels, in: Effects of Radiation on Materials: 18th International Symposium, in: R.K. Nanstad, M.L. Hamilton, F.A. Garner, A.S. Kumar (Eds.), ASTM STP 1325, American Society for Testing and Materials, West Conshohocken, PA, 1999, p. 167.
[29] Regulatory Guide 1.99 Revision 2, Radiation embrittlement of reactor vessel materials, Office of Nuclear Regulatory Research, US Nuclear Regulatory Commission, Washington, DC, May 1988.
[30] E.D. Eason, J.E. Wright, G.R. Odette, Improved embrittlement correlations for reactor pressure vessel steels, NUREG/CR-6551, US Nuclear Regulatory Commission, Washington, DC, 1998.
[31] ASTM E 900, Guide for predicting radiation-induced transition temperature shift in reactor vessel materials, E706 (IIF)Annual Book of ASTM Standards, vol. 12.02, American Society for Testing and Materials, West Conshohocken, PA, 2002.